Supporting Information

Ferroelasticity-like and solvent affect the magnetism of a copper-organic radical one-dimensional coordination polymer

Yan-Li Gao, [a] Sadafumi Nishihara, [b] Takashi Suzuki, [b] Kazunori Umeo, [b] Katsuya Inoue, *[b] and Mohamedally Kurmoo *[c]

[a] School of Chemistry and Chemical Engineering, Yulin University, Yulin 719000, China.

[b] Department of Chemistry and Center for Chiral Science, Hiroshima University, 1-3-1 Kagamiyama, Higashi-Hiroshima, Hiroshima, 739-8526 Japan.

[c] Institut de Chimie de Strasbourg, CNRS-UMR7177, Université de Strasbourg, 4 rue Blaise Pascal, 67070 Strasbourg, France.
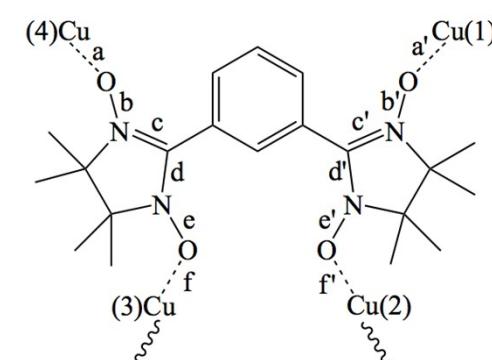
Table S1. Crystallographic and refinement data for **1·CH₂Cl₂**.

Crystal	AA	BB	CC
T (K)	296(2)	296(2)	100(2)
formula	$C_{51}H_{36}Cu_3F_{36}N_{16}O_{16}Cl_2$	$C_{51}H_{36}Cu_3F_{36}N_{16}O_{16}Cl_2$	$C_{51}H_{36}Cu_3F_{36}N_{16}O_{16}Cl_2$
fw	1906.4	1906.4	1906.4
cryst syst	Triclinic	Triclinic	Triclinic
space group	P -1	P -1	P -1
a (Å)	11.842(1)	11.831(1)	11.482(1)
b (Å)	12.992(1)	12.989(1)	12.833(1)
c (Å)	23.268(1)	23.257(1)	23.085(1)
α (°)	86.393(1)	86.396(1)	86.454(2)
β (°)	82.851(1)	82.885(1)	82.297(2)
γ (°)	86.258(1)	86.253(1)	86.259(2)
V (Å³)	3539.1(3)	3533.3(3)	3358.8(3)
Z	2	2	2
Refls. Total	94867	92780	120063
Unique	17492	17433	17182
Param.	1020	1020	1047
R_{int}	0.0248	0.0263	0.0401
R_1/wR_2	0.0578	0.0592	0.0448
$[I>2\sigma(I)]$	0.1627	0.1620	0.1153
R_1/wR_2	0.0784	0.0785	0.0561
(all data)	0.1816	0.1806	0.1215
GoF	1.042	1.048	1.096

Table S2. Crystallographic and refinement data for **1'**.

Crystal	**B**	**A**	**C**	**A**	**D**	**A**
T (K)	296(2)	200(2)	173(2)	130(2)	100(2)	85(2)
formula	$C_{25}H_{17}Cu_{1.5}F_{18}N_2O_8$	$C_{25}H_{17}Cu_{1.5}F_{18}N_2O_8$	$C_{25}H_{17}Cu_{1.5}F_{18}N_2O_8$	$C_{25}H_{17}Cu_{1.5}F_{18}N_2O_8$	$C_{25}H_{17}Cu_{1.5}F_{18}N_2O_8$	$C_{25}H_{17}Cu_{1.5}F_{18}N_2O_8$
fw	910.7	910.7	910.7	910.7	910.7	910.7
cryst syst	Monoclinic	Monoclinic	Monoclinic	Monoclinic	Monoclinic	Monoclinic
space group	$P\,2/n$	$P\,2/n$	$P\,2/n$	$P\,2/n$	$P\,2/n$	$P\,2/n$
a (Å)	13.936(1)	13.797(1)	13.742(1)	13.601(1)	13.488(1)	13.458(4)
b (Å)	16.422(1)	16.331(1)	16.308(1)	16.442(1)	15.967(1)	15.961(4)
c (Å)	16.492(1)	16.425(1)	16.436(1)	16.354(1)	17.039(1)	17.039(4)
α (°)	90.00	90.00	90.00	90.00	90.00	90.00
β (°)	97.969(1)	97.553(1)	97.467(2)	97.576(2)	95.059(2)	95.050(7)
γ (°)	90.00	90.00	90.00	90.00	90.00	90.00
V (Å^3)	3737.9(3)	3668.8(3)	3652.2(3)	3625.3(4)	3655.3(4)	3645.9(2)
Z	4	4	4	4	4	4
Refls. Total	59216	57238	55791	49552	51329	30545
Unique	9286	9137	9156	9021	9071	8933
Param.	498	498	498	498	498	498
R_{int}	0.0275	0.0253	0.0385	0.0394	0.0319	0.1053
R_1/wR_2	0.0719	0.0662	0.0670	0.0823	0.0902	0.1522
[I>2σ(I)]	0.2041	0.1843	0.1756	0.2372	0.2765	0.4142
R_1/wR_2	0.1010	0.0834	0.1016	0.1079	0.1100	0.2360
(all data)	0.2322	0.2035	0.2017	0.2673	0.3041	0.4716
GoF	1.050	1.032	1.026	1.051	1.038	1.545

Table S3. Intramolecular dimensions as a function of temperature for **1·CH₂Cl₂** and **1'**.

								1·CH₂Cl₂	
Crystal	T (K)	a (Å)	b (Å)	c (Å)	d (Å)	e (Å)	f (Å)	N4-O4-Cu4 (º)	N3-O2-Cu3 (º)
AA	296	2.032	1.292	1.344	1.352	1.271	2.711	121.48	144.81
BB	296	2.031	1.293	1.345	1.353	1.273	2.709	121.73	144.83
CC	100	1.999	1.297	1.353	1.358	1.277	2.653	120.77	142.64
		a' (Å)	b' (Å)	c' (Å)	d' (Å)	e' (Å)	f' (Å)	N1-O1-Cu1 (º)	N2-O2-Cu2 (º)
AA	296	2.263	1.289	1.338	1.357	1.276	2.642	126.80	154.36
BB	296	2.264	1.288	1.340	1.358	1.271	2.643	126.83	154.21
CC	100	2.258	1.295	1.349	1.363	1.276	2.559	125.81	155.87
								1'	
Crystal	T (K)	a (Å)	b (Å)	c (Å)	d (Å)	e (Å)	f (Å)	N2-O2-Cu2 (º)	N1-O1-Cu1 (º)
A	300	2.189	1.291	1.343	1.353	1.275	2.464	125.16	155.75
B	296	2.190	1.290	1.343	1.352	1.276	2.462	125.19	155.66
A	200	2.173	1.295	1.341	1.355	1.276	2.429	124.26	156.05
C	173	2.174	1.292	1.343	1.360	1.273	2.421	124.28	156.20
A	130	2.151	1.296	1.345	1.358	1.269	2.431	123.98	156.48
D	100	2.219	1.292	1.349	1.360	1.267	2.410	123.00	163.49
A	85	2.224	1.294	1.337	1.358	1.255	2.417	123.33	161.88

Thermogravimetric Analyses
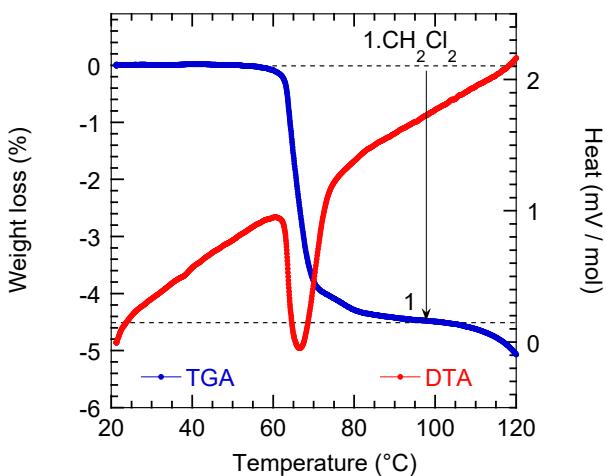
Figure S1. TG and DTA showing the transformation of **1·CH₂Cl₂** to **1**.

1·CH₂Cl₂ loses 4.3% of its weight at 65 °C (Figure S1), which corresponds to the departure of the CH_2Cl_2. The shiny black crystals used in this experiment crumbled into a dark green powder after heating to 100 °C.

Infrared Spectroscopy
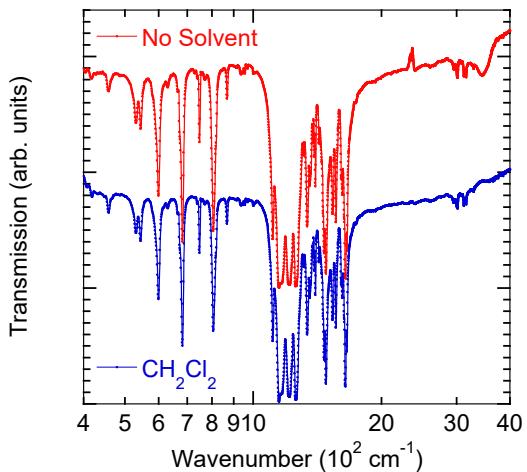
Figure S2. Infrared spectra of **1·CH₂Cl₂** and **1'**.

The infrared spectra of **1·CH₂Cl₂** and **1'** (Figure S2), which originate principally from the organic ligands, are almost identical with respect to the energies of the bands and their intensities. The result indicates that the ligands are not perturbed by the slight differences in structures. However, the lack of a solvent ν(C-Cl) band may indicate that the pressure used to make the KBr pellet has removed the solvent.

Crystal Structure
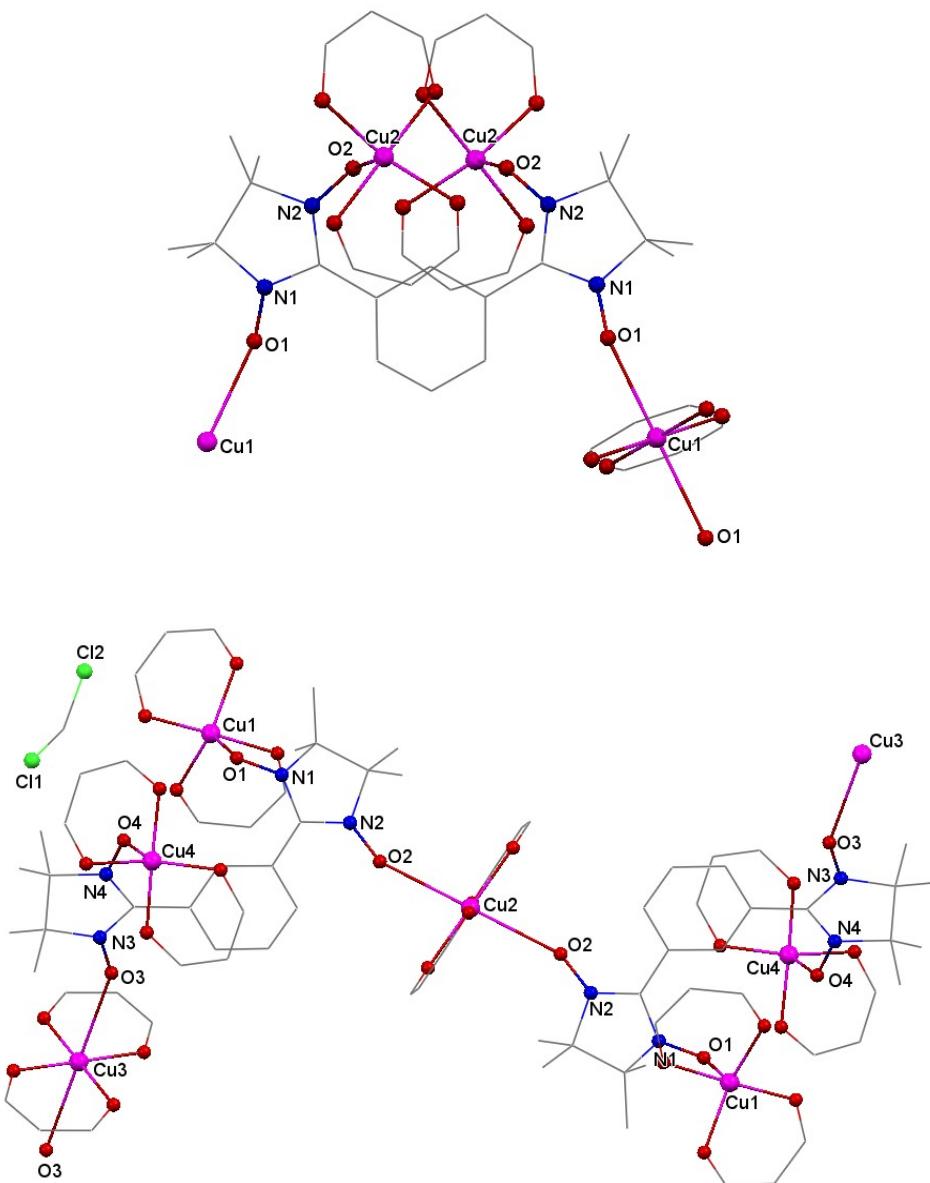
Figure S3. Fragment of molecular structure of $\{Cu^{II}(hfac)_2\}_3(m\text{-}BNN)\}$ (top) and $\{[Cu^{II}(hfac)_2]_3(m\text{-}BNN)]_n\} \cdot nCH_2Cl_2$ (below). Color codes for atoms: magenta spheres, Cu; Rred spheres, O; blue spheres, N; grey spheres, C; green spheres, Cl. All CF_3 groups and hydrogen atoms were omitted for the sake of clarity.

Figure S4. Details of the crystal packing of $\{Cu^{II}(hfac)_2\}_3(m\text{-BNN})\}$ (top) and $\{Cu^{II}(hfac)_2\}_3(m\text{-BNN})\cdot CH_2Cl_2\}$ (below). Color codes for atoms: magenta spheres, Cu; red spheres, O; blue spheres, N; grey spheres, C; green spheres, Cl. All CF_3 groups and hydrogen atoms were omitted for the sake of clarity.
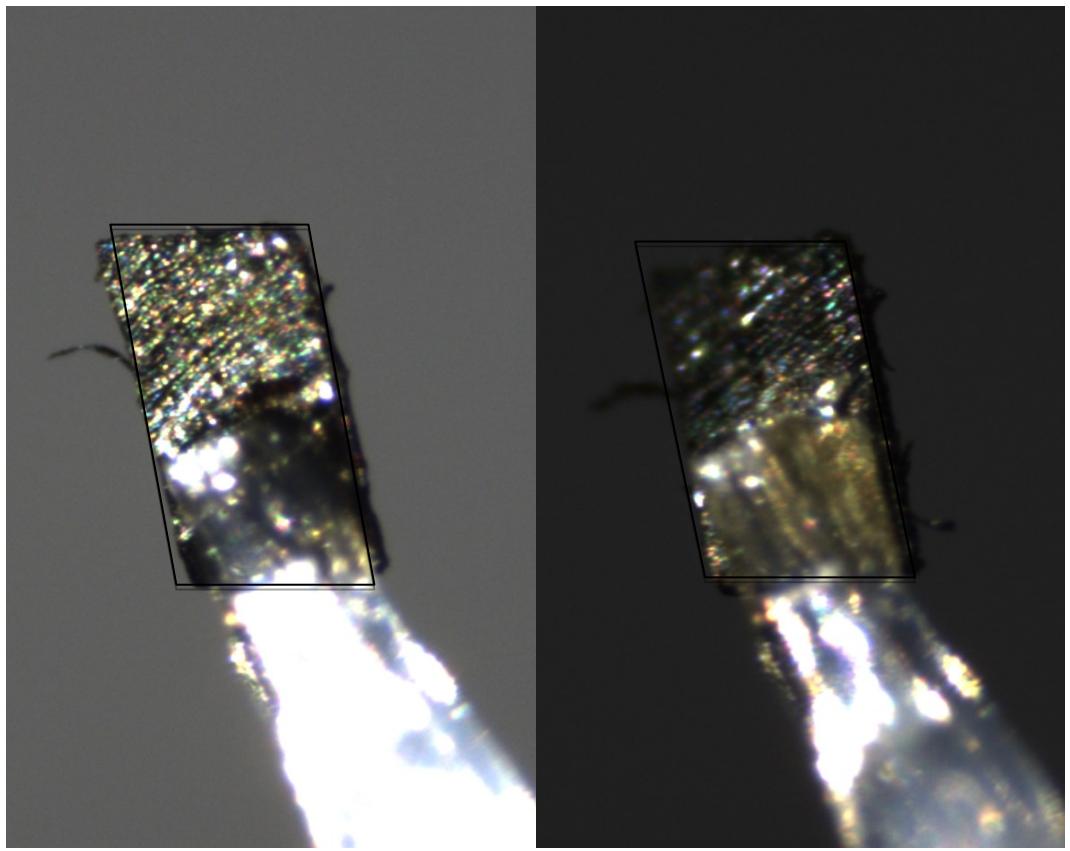
Figure S5. Top: Outline of the crystal (**1′**) at 110 K (yellow, left) and 100 K (red, right). Below: The shape change of the crystal.
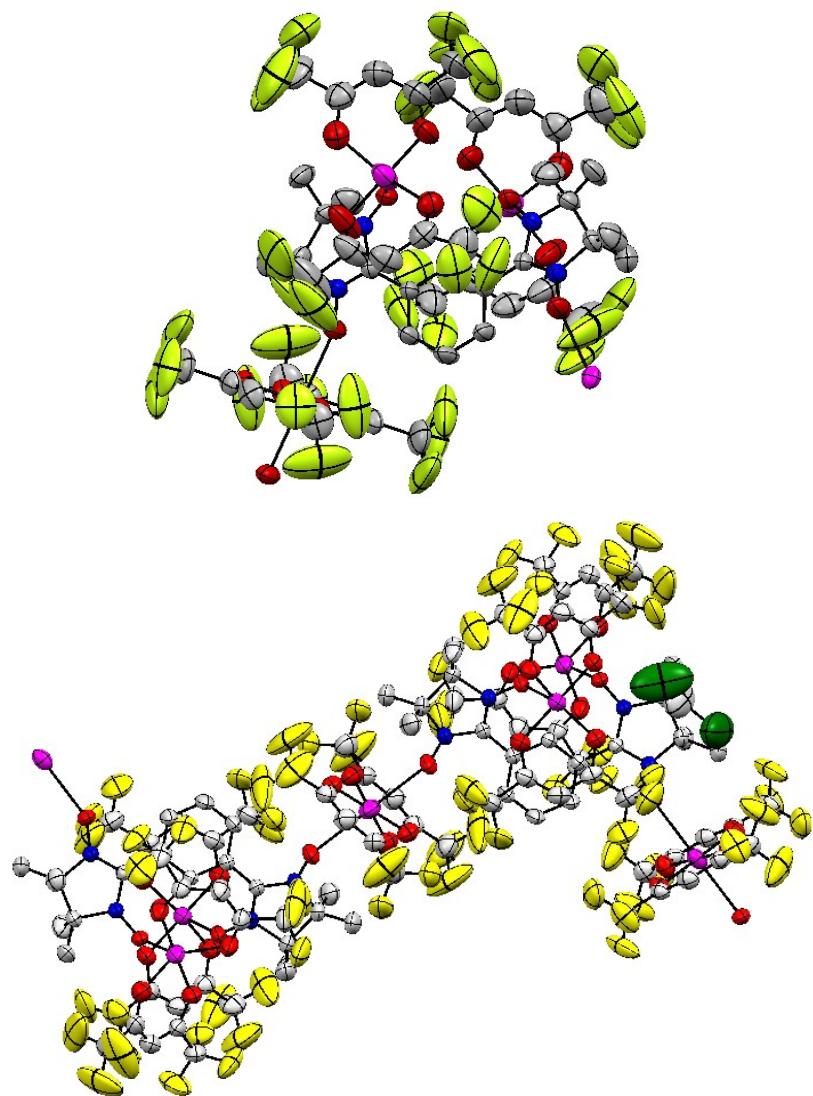
Figure S6. ORTEP view of the asymmetric unit of compounds $\{Cu^{II}(hfac)_2\}_3(m\text{-}BNN)\}$ (top) and $\{[Cu^{II}(hfac)_2]_3(m\text{-}BNN)]_n\}\cdot nCH_2Cl_2$ (below). ADPs at 50% probability. Color codes for atoms: magenta spheres, Cu; Rred spheres, O; blue spheres, N; grey spheres, C; yellow spheres, F; green spheres, Cl. All hydrogen atoms were omitted for the sake of clarity.

Magnetic Properties
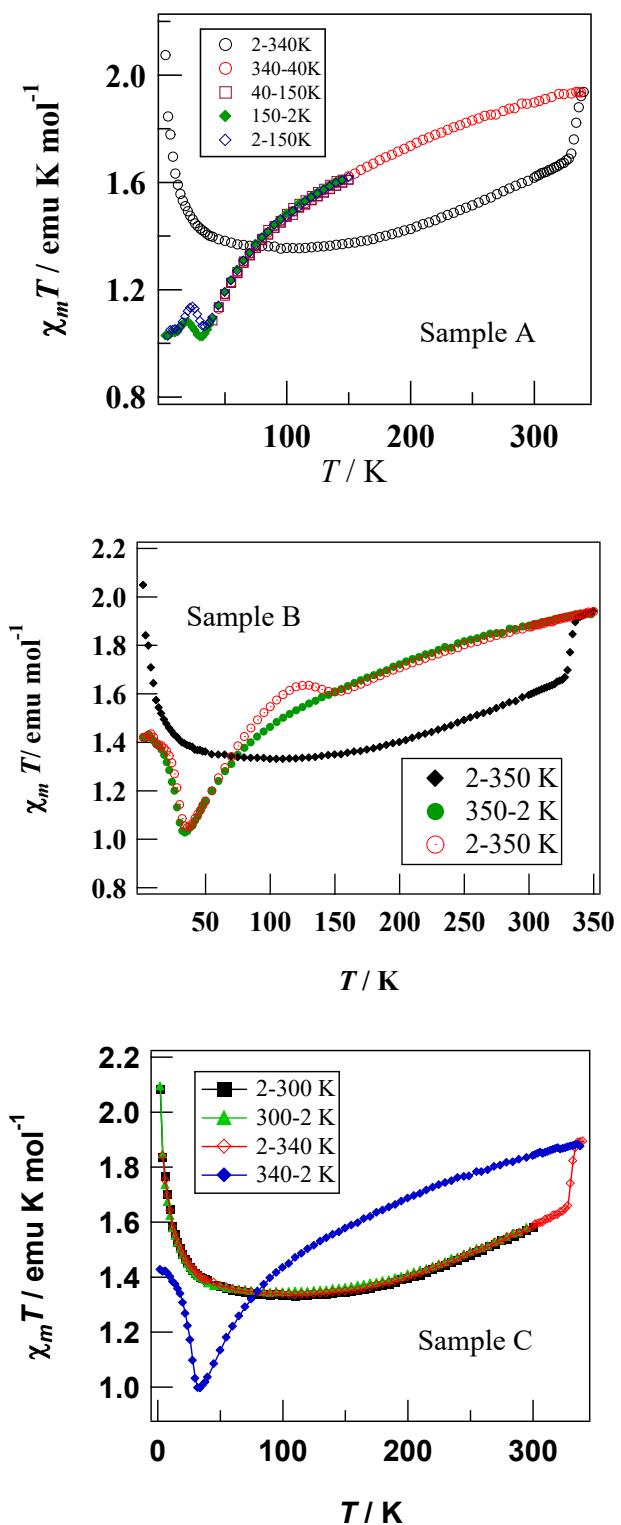
Figure S7. Temperature dependence of χT showing (top) the transformation of **1·CH₂Cl₂** to **1** at 335 K and the effect of temperature cycling for three samples (A, B and C) from different batches. Top, sample A, 2 → 340 → 40 → 150 → 2 → 150 K. Middle, sample B, 2 → 350 → 2 → 300→ 2 → 300 K. Below, sample C, 2 → 300 → 2 → 340 → 2 K.
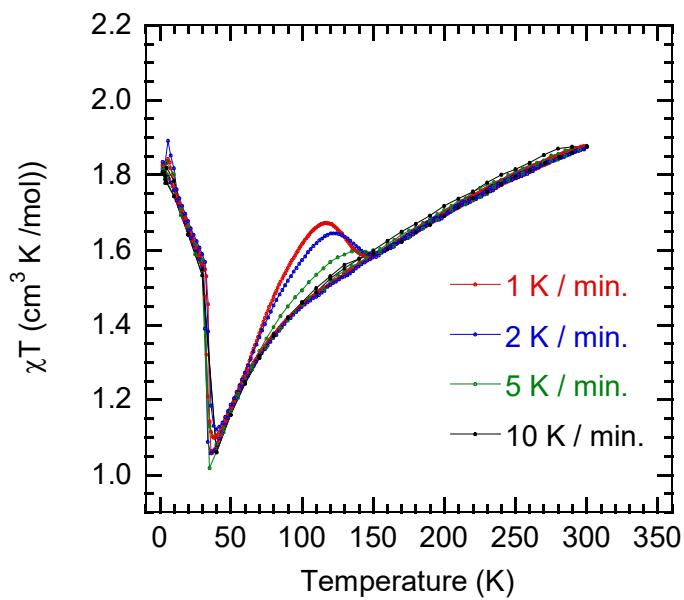
Figure S8. Temperature dependence of χT for **1'** as a function of heating and cooling rate. Note the hysteresis between 50 and 150 K for a slow rate of 1 K / min, decreasing progressively through 2, 5 and 10 K / min.
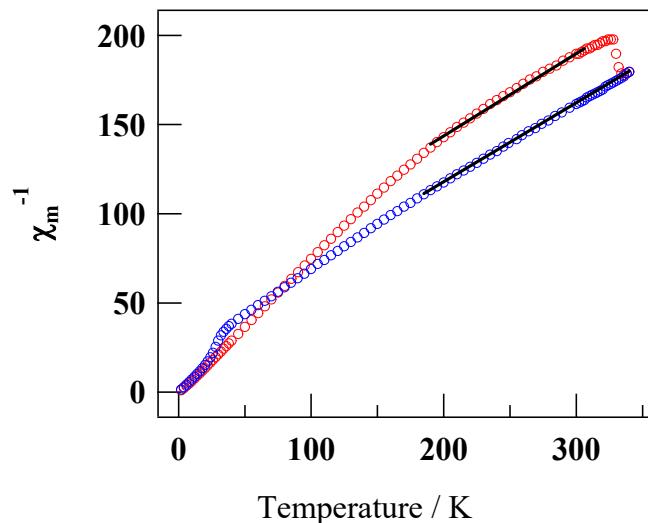

Figure S9. Temperature dependence of the product of magnetic susceptibility $\chi^{-1}(T)$ for **1·CH₂Cl₂** (red, 2 → 340 K; blue, 340 → 2 K)and Curie-Weiss fits(black).
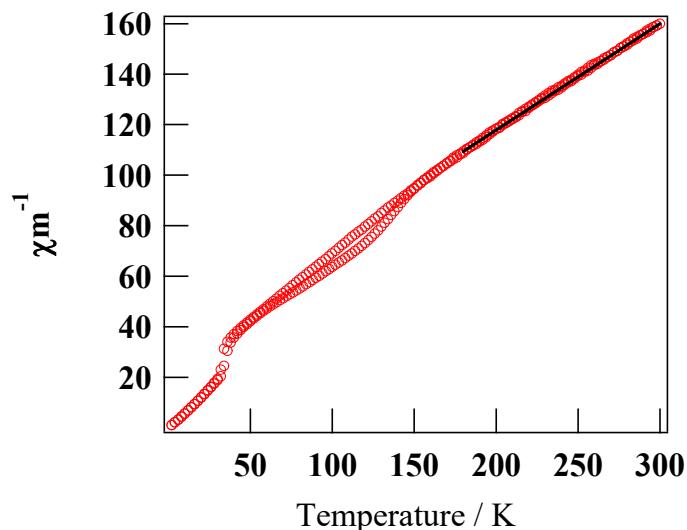
Figure S10. Temperature dependence of the product of magnetic susceptibility $\chi^{-1}(T)$ for **1′** (red) and Curie-Weiss fits(black).
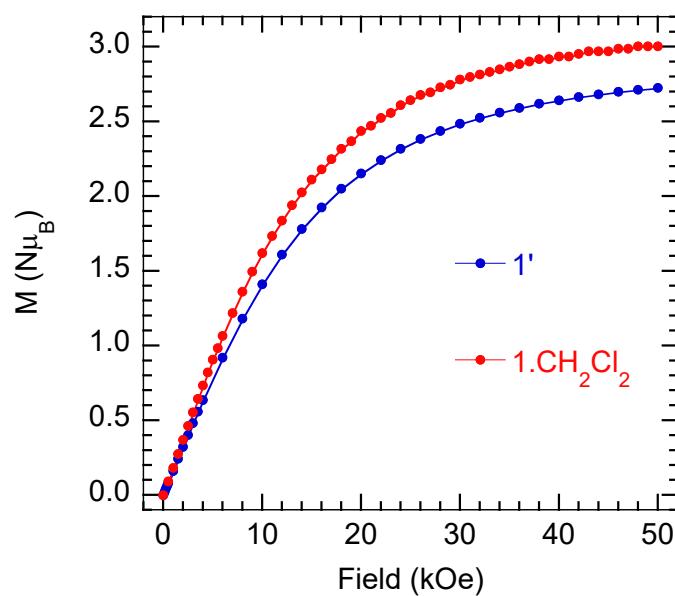

Figure S11. Isothermal magnetization at 2 K for **1·CH₂Cl₂** and **1'**.